A Multiple Shock Tube and Chemical Kinetic Modeling Study of Diethyl Ether Pyrolysis and Oxidation

K. Yasunaga,*,† F. Gillespie,† J. M. Simmie,† H. J. Curran,*,† Y. Kuraguchi,‡ H. Hoshikawa,‡ M. Yamane,‡ and Y. Hidaka‡

Combustion Chemistry Centre, School of Chemistry, NUI Galway, Ireland and Chemistry and Biology, Graduate School of Science and Engineering, Ehime University, Matsuyama, Japan

Received: May 4, 2010; Revised Manuscript Received: July 16, 2010

The pyrolysis and oxidation of diethyl ether (DEE) has been studied at pressures from 1 to 4 atm and temperatures of 900−1900 K behind reflected shock waves. A variety of spectroscopic diagnostics have been used, including time-resolved infrared absorption at 3.39 μm and time-resolved ultraviolet emission at 431 nm and absorption at 306.7 nm. In addition, a single-pulse shock tube was used to measure reactant, intermediate, and product species profiles by GC samplings at different reaction times varying from 1.2 to 1.8 ms. A detailed chemical kinetic model comprising 751 reactions involving 148 species was assembled and tested against the experiments with generally good agreement. In the early stages of reaction the unimolecular decomposition and hydrogen atom abstraction of DEE and the decomposition of the ethoxy radical have the largest influence. In separate experiments at 1.9 atm and 1340 K, it is shown that DEE inhibits the reactivity of an equimolar mixture of hydrogen and oxygen (1% of each).

Introduction

To reduce the use of fossil fuels, biofuels have attracted considerable attention. Ethanol is at present the most widely used spark-ignited biofuel because of its high octane number. Diethyl ether (DEE) is easily produced through the dehydration of ethanol. In order to evaluate the viability of DEE as a transportation fuel, Bailey et al.[1] reported on several favorable properties, including a cetane number of higher than 125[2] and a boiling point of 34 °C. There is little previous work on the pyrolysis and oxidation of DEE in the literature. Laidler et al.[3,4] measured the rate of pyrolysis of DEE at temperatures from 560 to 630 °C at pressures from 15 to 320 mmHg and determined all bimolecular rate constants to be: $k_{668} = 1.0 \times 10^{14} \exp(-39\,250/T)$, $k_{670} = 1.0 \times 10^{18} \exp(-42\,270/T)$, and $k_{677+678} = 1.0 \times 10^{11} \exp(-5030/T)$ cm^3 mol^{-1} s^{-1}, respectively.

$$\mathrm{DEE} + \mathrm{M} = \mathrm{C_2H_5\dot{O}} + \mathrm{\dot{C}_2H_5} + \mathrm{M} \qquad (668)$$

$$\mathrm{DEE} + \mathrm{M} = \mathrm{C_2H_5OH} + \mathrm{C_2H_4} + \mathrm{M} \qquad (670)$$

$$\mathrm{DEE} + \mathrm{\dot{C}H_3} = \mathrm{C_2H_5O\dot{C}_2H_4\text{-}p} + \mathrm{CH_4} \qquad (677)$$

$$\mathrm{DEE} + \mathrm{\dot{C}H_3} = \mathrm{C_2H_5O\dot{C}_2H_4\text{-}s} + \mathrm{CH_4} \qquad (678)$$

Seres et al.[5] measured rate constants for the unimolecular decomposition reactions to be $k_{668} = 2.0 \times 10^{14} \exp(-39\,000/T)$ s^{-1} and $k_{670} = 7.9 \times 10^{13} \exp(-33\,200/T)$ s^{-1}. Foucaut et al.[6] also measured these as $k_{668} = 2.5 \times 10^{15} \exp(-38\,600/T)$ s^{-1} and $k_{670} = 1.0 \times 10^{13} \exp(-31\,300/T)$ s^{-1}.

* To whom correspondence should be addressed. E-mail: kenji.yasunaga@nuigalway.ie (K. Y.), henry.curran@nuigalway.ie (H. J. C.).
† NUI Galway.
‡ Ehime University.

TABLE 1: Composition of Mixtures (mol %)

mixture	DEE	O_2	H_2	Ar
A	2.0			98.0
B	1.0	3.0		96.0
C	1.0	6.0		93.0
D	1.0	12.0		87.0
E	0.1	1.0	1.0	97.9

Waddington[7] studied the oxidation of DEE at 153 °C and found that the induction period of DEE and oxygen mixtures depends on both of their initial concentrations. Tranter et al.[8] estimated the rate of DEE + Ḣ, and DEE + ȮH reactions at 753 K, measuring the pressure variation of DEE, O_2, and H_2 mixtures. Ogura et al.[9] calculated the rate constants of hydrogen atom abstraction from the carbon adjacent to oxygen by Ḣ atom and ȮH radical for several ethers.

There has been much work recently on the combustion characteristics of DEE,[10−14] but none that has impinged on the chemical kinetics of this system. In the present work, we have carried out pyrolysis and oxidation experiments behind reflected shock waves and constructed a detailed chemical reaction model to describe these.

Experimental Section

Samples of DEE fuels 99.9% and 99.0% pure were supplied by Sigma-Aldrich and Wako Pure Chemical, and degassed through a series of freeze−thaw-pump cycles, after which no more gas was observed to escape on thawing the solid. The oxygen 99.5% and 99.999% were supplied by BOC and Taiyotoyosanso Co. The argon 99.9% and 99.999% were supplied by BOC and Teisan Co. Mixtures were prepared using the method of partial pressures and their compositions are provided in Table 1. The incident shock velocity at the end wall was used to calculate the temperature and pressures of the mixture behind the reflected shock wave using the equilibrium program Gaseq.[15]

10.1021/jp104070a
Published on Web 08/06/2010

Four shock tubes, of which surfaces of the inner reaction sections are unpolished, were used in this study, the first three described herein are based at Ehime University in Japan, and the fourth resides at NUI Galway. The first shock tube (Single Pulse Shock Tube: SPST) with 4.1 cm i.d. was a magic-hole-type. A simple description is only given below, since the apparatus has been described in detail previously by Hidaka et al.[16−19] The reacted gas mixtures quenched using the single pulse method were extracted into a pre-evacuated vessel (50 cm^3) through a valve near the end plate. The reacted gas mixtures were analyzed by three serially connected gas chromatographs each having a thermal conductivity detector (TCD).[18,19] The gas chromatographic analyses were carried out as follows. Shimadzu GC-8A with 2 m column packed with Sebaconitrile and heated to 75 °C was used to determine concentrations of DEE, C_2H_5OH, CH_3CHO, and hydrocarbons above C_4. Shimadzu GC-8A2 with 2 m column packed with Porapak Q connected to a 2 m column packed with Unibeads 1S was used to determine the concentrations of C_2H_6, C_2H_4, C_2H_2, C_3H_8, C_3H_6, C_3H_4-a (allene), C_3H_4-p (propyne) and CO_2, heating these columns at a rate of 3 °C/min from 50 to 130 °C. Shimadzu GC-3BT with 2 m column packed with Molecular Sieve 5A at 50 °C was used to determine the concentrations of CH_4 and CO. Helium was used as a carrier gas. The output signal from each gas chromatograph was introduced into Shimadzu Chromatopac C-R3A1, C-R3A2, and C-R1B data processors. An effective heating time, t_e, (reaction time), which was defined as the time between the arrival of the reflected shock wave and the point at which the reflected shock pressure had fallen by 20%, was determined with an accuracy of ±5% using the method described previously.[17,18] Assuming that the adiabatic expansion of nonreactive mixture, temperature drops by 8.5% from initial value at effective heating time.

Given that single pulse shock tubes have cooling rates of 6.6×10^5 K s^{-1},[16] it can be assumed that the reaction was frozen at the effective heating time, the concentrations of carbon-containing compounds and hydrogen, determined by gas chromatography, were compared with those from the simulation. The validity of effective heating time and cooling rate was tested for N_2O pyrolysis previously.[16] The experimental uncertainties of the concentrations are less than 2% except for C_2H_5OH due to strong adsorption. The estimated experimental uncertainty of the concentration of C_2H_5OH was less than ±30%.

The second shock tube (Laser Absorption Shock Tube: LAST) with 4.1 cm i.d. was a standard-type connected to laser absorption equipment.[20,21] The transmitted intensity of a 3.39 μm He−Ne laser beam through a 4.1 cm path-length in the shock tube passed through an interference filter (λ_{max} = 3.39 μm, half-width = 0.072 μm) was monitored with an InSb detector using the same method as described previously.[20,21] The wavelength 3.39 μm (≈3000 cm^{-1}) corresponds to C−H stretch, so that 3.39 μm laser beam is absorbed by many hydrocarbon compounds, but mainly by DEE under our experimental conditions. The decay rates of absorbance profiles reflect that of DEE. The extinction coefficients for the reactant and products measured previously[20−22] were used in the simulations. A_t is defined by the following equation: $A_t = \log (I_f/I_t)/\log (I_f/I_0)$, where I_f corresponds to the incident light intensity and I_0 and I_t corresponds to the transmitted light intensity at the reflected shock front ($t = 0$) and at time t, respectively. The relationship between the extinction coefficient and temperature T was calculated from the observed reflected shock absorption profiles. The equation for the extinction coefficient for DEE was I_a (DEE) $= 1.0 \times 10^4 - 28.4 \times T$ cm^2 mol^{-1}.

Moreover, the extinction coefficients for products that have a C−H bond were measured using mixtures, 5% C_2H_5OH, 4% C_3H_4-a, 4% C_3H_4-p, 4% C_3H_6, 1% CH_3CHO, 2% C_2H_6, 6% C_2H_4, 6% C_2H_2, and 5% CH_4, respectively, diluted in Ar. The equations for the extinction coefficients obtained for these species were: $I_a(C_2H_5OH) = 4.83 \times 10^3 - 19.0 \times T$ cm^2 mol^{-1}, $I_a(C_3H_4\text{-a}) = 2.2 \times 10^3 - 0.44 \times T$ cm^2 mol^{-1}, $I_a(C_3H_4\text{-p}) = 1.07 \times 10^4 - 3.00 \times T$ cm^2 mol^{-1}, $I_a(C_3H_6) = 2.86 \times 10^4 - 7.8 \times T$ cm^2 mol^{-1}, $I_a(CH_3CHO) = 5.20 \times 10^3$ cm^2 mol^{-1}, $I_a(C_2H_6) = 5.43 \times 10^4 - 17.5 \times T$ cm^2 mol^{-1}, $I_a(C_2H_4) = 3.38 \times T$ cm^2 mol^{-1}, $I_a(C_2H_2) = -1.44 \times 10^3 + 1.03 \times T$ cm^2 mol^{-1}, and $I_a(CH_4) = 3.46 \times 10^4 - 16.7 \times T$ cm^2 mol^{-1} ($T \le 1604$ K) or $I_a(CH_4) = 1.18 \times 10^4 - 2.51 \times T$ cm^2 mol^{-1} ($T > 1604$ K), respectively. These were determined within an uncertainty of ±5% used in the simulations.

The third shock tube (UV Absorption Shock Tube: UAST) with 4.1 cm i.d. was a standard-type connected to UV absorption equipment.[21] A light at 306.7 nm from a microwave discharge of H_2O in He through a 4.1 cm path-length in the shock tube, dispersed by a grating monochromator, was monitored with a photomultiplier, using the same method as described previously.[16,19,21] The extinction coefficient of the ȮH radical at 306.7 nm used in the simulation is $10^{-3.51\times T+7.3}$ cm^2 mol^{-1}, which was estimated from the partial equilibrium of ȮH radical in the 1.0% H_2, 1.0% O_2 mixture diluted with Ar.

The fourth shock tube (UV Emission Shock Tube: UEST), also a standard-type based at NUI Galway, consists of a test section measuring 6.22 m in length, with an internal diameter of 10.24 cm, and a barrel-shaped driver section measuring 53 cm in length. The two sections are separated by a polycarbonate diaphragm, which burst when forced into contact with a cross-shaped cutter due to the pressure differential. Four pressure transducers located along the last half meter of the tube were used to determine the velocity of the incident shock wave. The velocity at the endwall was determined through linear extrapolation, so as to take attenuation of the shock wave into account.

The pressure at the endwall was monitored by a pressure transducer (Kistler, model 603B). Light emission at 431 nm, which is emitted from excited CH* radicals, was detected through a fused silica window embedded in the end-plate using a photodetector (Thorlabs Inc. PDA55-EC) and a narrow band-pass filter centered at 430 nm with a full-width half-maximum of 10 nm. The ignition delay time was defined as the interval between the rise in pressure due to the arrival of the shock wave at the endwall and the maximum rate of rise of the emission signal.

Model. The thermodynamic data for DEE was calculated using the THERM program of Ritter and Bozzelli,[23] based on the group additivity methods developed by Benson,[24] and are provided in Table 2. These data are in agreement with recommendation in the NIST WebBook.[25] The $C_2H_5O\dot{C}_2H_4$-s radical is formed via abstraction of a (secondary) hydrogen atom α to the oxygen atom in DEE, whereas the $C_2H_5O\dot{C}_2H_4$-p results from (primary) hydrogen atom abstraction β to the oxygen atom. The reaction mechanism is available online at http://c3.nuigalway.ie/mechanisms.html.

Unimolecular Decomposition. The DEE submechanism includes the two possible classes of unimolecular decomposition reaction, including simple and complex fission.

$$DEE + M = C_2H_5\dot{O} + \dot{C}_2H_5 + M \qquad (668)$$

TABLE 2: Thermochemical Data of DEE and Related Radicals

	ΔH_f° (298.15 K) (kcal/mol)	S° (298.15 K) (cal/(mol K))	C_p (cal/(mol K))				
			300 K	500 K	800 K	1000 K	1500 K
DEE	−60.44	81.87	25.77	39.01	52.61	58.80	68.38
DEE[a]	−60.40	81.79	28.65	39.62	52.59	58.72	68.30
$C_2H_5O\dot{C}_2H_4$-s	−17.93	84.87	24.94	38.21	50.24	55.57	63.89
$C_2H_5O\dot{C}_2H_4$-p	−11.84	86.66	25.00	37.10	49.45	55.06	63.72
$C_2H_5O\dot{C}H_2$	−8.78	75.20	20.47	30.04	39.49	43.64	49.98

[a] The recommendation values of NIST.[25]

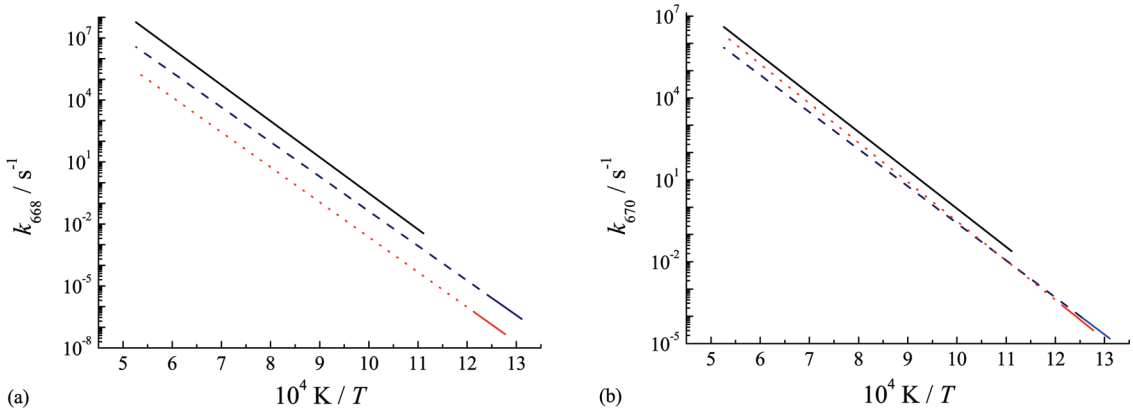

Figure 1. Comparison of the rate constants to literature value: (a) reaction 668: (b) reactions 670. Solid lines, this study; dotted lines connected to solid lines, Seres et al.;[5] dashed lines connected to solid lines, Foucaut et al.[6] Solid lines covers the temperature range at which rate constants were estimated.

$$DEE + M = C_2H_5O\dot{C}H_2 + \dot{C}H_3 + M \qquad (669)$$

The high pressure limit rate constants for each of these simple fission reactions were calculated based on microscopic reversibility using an estimate of the rate constant in the reverse direction for radical−radical recombination. For reaction (−668) a rate constant of 3.0×10^{13} cm^3 mol^{-1} s^{-1} was used similar to that for methoxy radical recombination with methyl radical.[26] For reaction (−669) a rate constant of 2.0×10^{13} cm^3 mol^{-1} s^{-1} was used as recommended by Tsang[27] for recombination of ethyl and n-propyl radicals to form n-pentane. The estimated rate constant for reaction 668 is compared to literature values[5,6] in Figure 1a. Our value is approximately 8 and 15 times faster those of Foucaut et al. and Seres et al. at 1000 K, and approximately 15 and 240 times faster at 1900 K, respectively. As a complex fission, the four-centered elimination to ethanol and ethylene was considered.

$$DEE + M = C_2H_5OH + C_2H_4 + M \qquad (670)$$

The high pressure limit rate constant of $1.0 \times 10^{14}\exp(-32\,335/T)$ s^{-1} was adopted for reaction 670. This is estimated by analogy with the unimolecular elimination reaction of ethyl *tert*-butyl ether (ETBE) as described by Yasunaga et al.,[28] who showed that not only does ETBE undergo a four-centered elimination to form *iso*-butene and ethanol, reaction E1, but also undergoes a similar elimination to form *tert*-butanol and ethylene, reaction E2.

$$ETBE = iC_4H_8 + C_2H_5OH \qquad (E1)$$

$$ETBE = (CH_3)_3COH + C_2H_4 \qquad (E2)$$

Taking into account the number of methyl groups in DEE, double the value of the frequency factor proposed by Yasunaga et al. for reaction E2 was adopted for reaction 670. An activation energy of 65.21 kcal mol^{-1} was used, which was calculated using Gaussian 03 program package[29] at the MP4/cc-pVTZ//MP2/cc-pVTZ level of theory. This rate constant of reaction 670 is approximately three times faster than that of Foucaut et al. over their limited temperature range of 763−798 K. Our rate constant is also approximately two times faster than the value of Seres et al. at 1000 K, and 1.5 times faster at 1900 K, Figure 1b. A chemical activation formulation based on Quantum Rice−Ramsperger−Kassel (QRRK) theory, as described by Dean[30,31] was then used together with the high pressure limit expressions to develop pressure-dependent rate constants which were fit to a nine-parameter Troe formalism.[32]

Hydrogen Abstraction. Rate constants for hydrogen abstraction by $\dot{H}$, $\dot{C}H_3$, and $\dot{O}H$ radicals from the α and β positions were considered in this study. The rate constants for hydrogen abstraction by $\dot{H}$ and $\dot{O}H$ radicals from the α position were taken from the work of Ogura et al.[9] and Zhou et al.,[33] whereas that for abstraction by $\dot{C}H_3$ radicals was from Orme et al.[34] by analogy with secondary hydrogen atom abstraction from an alkane. Those for abstraction by $\dot{H}$ atom $\dot{O}H$ and $\dot{C}H_3$ radicals from the β position were taken to be analogous to primary hydrogen atom abstraction from an alkane and were also taken from the work of Orme et al.[34] These rate constants are provided in Table 3.

Radical Decomposition. The $C_2H_5O\dot{C}_2H_4$-p, $C_2H_5O\dot{C}_2H_4$-s, and $C_2H_5O\dot{C}H_2$ radicals are produced through the pyrolysis and oxidation of DEE. These radicals mainly decompose via β-scission at temperatures above approximately 1000 K. We considered reactions 718, 719 and 749 in the reverse, exothermic direction, as the addition of an alkyl radical to a C═O and C═C

TABLE 3: Elementary Reactions and Rate Constant Expressions. Rate Constants in the Form, $AT^n \exp(-E_a/RT)$, in cm^3, mol, cal, and K[a]

No.	reaction	A	n	E_a	ref.
(668)	DEE = $C_2H_5\dot{O}$ + $\dot{C}_2H_5$	$k_\infty = 1.24 \times 10^{25}$	−2.29	85 330	This work
		$k_0 = 3.55 \times 10^{83}$	−18.7	98 640	
	troe parameters: 9.0×10^{-06}, 506, 1.41×10^{10}, 2470				
(669)	DEE = $\dot{C}H_2OC_2H_5$ + $\dot{C}H_3$	$k_\infty = 2.80 \times 10^{22}$	−1.59	88 400	This work
		$k_0 = 7.95 \times 10^{78}$	−17.5	99 510	
	troe parameters: 0.091, 437, 2.63×10^7, 2833				
(670)	DEE = C_2H_5OH + C_2H_4	$k_\infty = 1.0 \times 10^{14}$	0.00	65 210	This work
		$k_0 = 5.72 \times 10^{96}$	−23.0	80 813	
	troe parameters: 1.17×10^{-3},379, 1.58×10^7,4730				
(681)	DEE + $\dot{H}$ = $C_2H_5O\dot{C}_2H_4$-p + H_2	1.32×10^6	2.54	6760	34
(682)	DEE + $\dot{H}$ = $C_2H_5O\dot{C}_2H_4$-s + H_2	2.60×10^6	2.40	4470	9
(677)	DEE + $\dot{C}H_3$ = $C_2H_5O\dot{C}_2H_4$-p + CH_4	9.03×10^{-01}	3.65	7150	34
(678)	DEE + $\dot{C}H_3$ = $C_2H_5O\dot{C}_2H_4$-s + CH_4	$3.01 \times 10°$	3.46	5480	34
(673)	DEE + $\dot{O}H$ = $C_2H_5O\dot{C}_2H_4$-p + H_2O	9.06×10^{-01}	3.65	7421	34
(674)	DEE + $\dot{O}H$ = $C_2H_5O\dot{C}_2H_4$-s + H_2O	2.26×10^3	2.93	4040	33
(675)	DEE + $H\dot{O}_2$ = $C_2H_5O\dot{C}_2H_4$-p + H_2O_2	5.52×10^4	2.55	16500	34
(676)	DEE + $H\dot{O}_2$ = $C_2H_5O\dot{C}_2H_4$-s + H_2O_2	2.95×10^4	2.60	13 900	34
(679)	DEE + $\ddot{O}$ = $C_2H_5O\dot{C}_2H_4$-p + $\dot{O}H$	1.96×10^6	2.43	4750	34
(680)	DEE + $\ddot{O}$ = $C_2H_5O\dot{C}_2H_4$-s + $\dot{O}H$	1.10×10^6	2.45	2830	34
(719)	$C_2H_5O\dot{C}_2H_4$-s = $\dot{C}_2H_5$ + CH_3CHO	2.86×10^{15}	−0.24	10 165	This work
(718)	$C_2H_5O\dot{C}_2H_4$-p = $C_2H_5\dot{O}$ + C_2H_4	2.28×10^{11}	0.67	23 501	This work
(749)	$C_2H_5O\dot{C}H_2$ = $\dot{C}_2H_5$ + CH_2O	3.29×10^{15}	−0.27	13 137	This work

[a] The Troe parameters are listed in the order: a, T^*, T^{***}, T^{**}.

moiety. These rate constants were estimated based on the recommendation of Curran.[35]

$$C_2H_5O\dot{C}_2H_4\text{-s} = \dot{C}_2H_5 + CH_3CHO \qquad (719)$$

$$C_2H_5O\dot{C}_2H_4\text{-p} = C_2H_5\dot{O} + C_2H_4 \qquad (718)$$

$$C_2H_5O\dot{C}H_2 = \dot{C}_2H_5 + CH_2O \qquad (749)$$

For reaction (−718) and (−719) a rate constant of 8.80×10^{03} $T^{2.48}$ exp(−3085/T) cm^3 mol^{-1} s^{-1} was estimated. For reaction (−749) a value of 1.32×10^{04} $T^{2.48}$ exp(−3085/T) cm^3 mol^{-1} s^{-1} was used. Rate constants for these alkyl radical decompositions are provided in Table 3.

Submechanism. Hydrogen atom abstraction reaction from acetaldehyde by hydrogen atoms at the α-position is an important reaction in the pyrolysis and oxidation of DEE, we adopted the rate constant based on the work of Bentz et al.,[36] who used shock tube experiments coupled with the H-ARAS technique. The submechanism of C1−C4 hydrocarbon chemistry is the same as the recent natural gas,[37−42] *n*-butane[43] and *iso*-butane[44] mechanisms and their blends[45] published from this laboratory.

Comparison to Experiment. Simulations were performed using Chemkin-Pro,[46] using the closed homogeneous batch reactor model at constant volume for our shock tube experiments.

Pyrolysis. ***Species Profiles.*** The species profiles were measured using the SPST. Major species profiles were simulated for mixtures of 2% DEE diluted with argon in the pressure range 1.0−3.1 atm with effective heating times in the range 1.2−1.8 ms. Effective heating times decrease as the shock velocity increases, which results in higher temperatures. Hence, heating times decrease as the temperature increases. The result is shown in Figure 2. The concentration of DEE begins to decrease at 1000 K. The concentrations of ethanol, acetaldehyde and propane increase as the temperature rises to approximately 1300 K and then decreases. The concentrations of ethane, ethylene, and propene increase to approximately 1450 K and then decrease. The concentration of allene increases to approximately 1500 K and then decrease. The concentrations of methane, carbon monoxide, acetylene, and propyne simply increase as temperature rises under our experimental conditions. The model captures well these species versus temperature profiles. DEE decompose via unimolecular reactions and hydrogen abstraction reactions by $\dot{H}$ atom and $\dot{C}H_3$ radical.

$$DEE(+M) = \dot{C}_2H_5 + C_2H_5C\dot{O}(+M) \qquad (668)$$

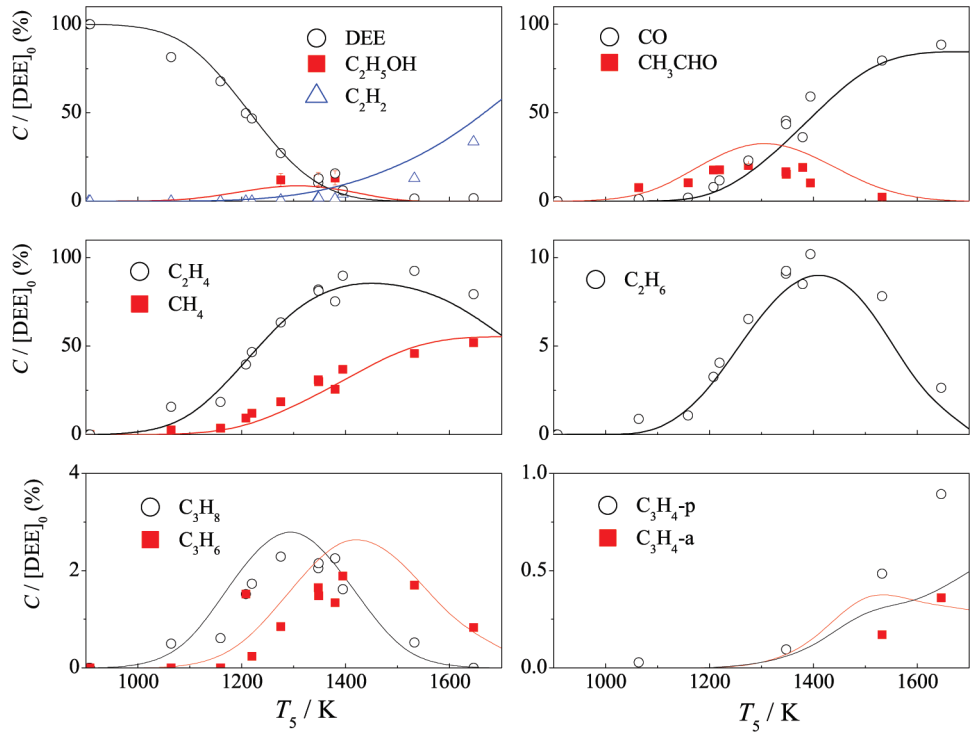

Figure 2. Species profiles from SPST for 2.0% DEE diluted in Ar at 1.0−2.9 atm; lines are simulation and symbols are experiment. $[DEE]_0$ and C denote initial concentration of DEE and concentration of chemical species after shock heated. Effective heating times used at 900, 1000, 1100, 1200, 1300, 1400, 1500, 1600, and 1700 K were 1800, 1730, 1650, 1580, 1500, 1430, 1350, 1200, and 1200 μs, respectively.

$$DEE(+M) = C_2H_5O\dot{C}H_2 + \dot{C}H_3(+M) \quad (669)$$

$$DEE(+M) = C_2H_5OH + C_2H_4(+M) \quad (670)$$

$$DEE + \dot{H} = C_2H_5O\dot{C}_2H_4\text{-p} + H_2 \quad (681)$$

$$DEE + \dot{H} = C_2H_5O\dot{C}_2H_4\text{-s} + H_2 \quad (682)$$

$$DEE + \dot{C}H_3 = C_2H_5O\dot{C}_2H_4\text{-p} + CH_4 \quad (677)$$

$$DEE + \dot{C}H_3 = C_2H_5O\dot{C}_2H_4\text{-s} + CH_4 \quad (678)$$

Ethanol is produced via reaction 670 and decomposes mainly via unimolecular decomposition reactions and hydrogen abstraction reactions by $\dot{H}$ atom and $\dot{C}H_3$ radical.

$$C_2H_5OH(+M) = \dot{C}H_2OH + \dot{C}H_3(+M) \quad (280)$$

$$C_2H_5OH(+M) = C_2H_4 + H_2O(+M) \quad (282)$$

$$C_2H_5OH + \dot{H} = \dot{C}_2H_4OH\text{-p} + H_2 \quad (289)$$

$$C_2H_5OH + \dot{H} = \dot{C}_2H_4OH\text{-s} + H_2 \quad (290)$$

$$C_2H_5OH + \dot{H} = C_2H_5\dot{O} + H_2 \quad (291)$$

$$C_2H_5OH + \dot{C}H_3 = \dot{C}_2H_4OH\text{-p} + CH_4 \quad (301)$$

$$C_2H_5OH + \dot{C}H_3 = \dot{C}_2H_4OH\text{-s} + CH_4 \quad (302)$$

$$C_2H_5OH + \dot{C}H_3 = C_2H_5\dot{O} + CH_4 \quad (303)$$

Acetaldehyde is principally produced via unimolecular decomposition of $C_2H_5O\dot{C}_2H_4$-s radical and ethoxy radical produced by reactions 678, 682, and 668, and decomposes mainly via hydrogen abstraction reactions by $\dot{H}$ atom and $\dot{C}H_3$ radical.

$$C_2H_5O\dot{C}_2H_4\text{-s} = CH_3CHO + \dot{C}_2H_5 \quad (719)$$

$$C_2H_5\dot{O} = CH_3CHO + \dot{H} \quad (175)$$

$$CH_3CHO + \dot{H} = CH_3\dot{C}O + H_2 \quad (207)$$

$$CH_3CHO + \dot{C}H_3 = CH_3\dot{C}O + CH_4 \quad (211)$$

Ethane is mainly produced via recombination reaction of methyl radicals, and mainly decomposes via hydrogen abstraction reactions by $\dot{H}$ and $\dot{C}H_3$.

$$\dot{C}H_3 + \dot{C}H_3(+M) = C_2H_6(+M) \quad (151)$$

$$C_2H_6 + \dot{H} = \dot{C}_2H_5 + H_2 \quad (153)$$

$$C_2H_6 + \dot{C}H_3 = \dot{C}_2H_5 + CH_4 \quad (157)$$

Ethylene is principally produced via unimolecular elimination reactions 670 and 282 (the unimolecular decomposition of ethyl radical) and $C_2H_5O\dot{C}_2H_4$-p radical produced by reactions 677 and 681, and mainly decomposes via hydrogen abstraction reactions by $\dot{H}$ and $\dot{C}H_3$, and methyl radical addition to produce propene and H atom.

$$C_2H_4 + \dot{H}(+M) = \dot{C}_2H_5(+M) \quad (163)$$

$$C_2H_5O\dot{C}_2H_4\text{-p} = C_2H_4 + C_2H_5\dot{O} \quad (718)$$

$$C_2H_4 + \dot{H} = \dot{C}_2H_3 + H_2 \quad (248)$$

$$C_2H_4 + \dot{C}H_3 = \dot{C}_2H_3 + CH_4 \quad (252)$$

$$C_3H_6 + \dot{H} = C_2H_4 + \dot{C}H_3 \quad (461)$$

Propane is produced via methyl and ethyl radicals association reaction and mainly decomposes via hydrogen abstraction reactions by $\dot{H}$ and $\dot{C}H_3$ radicals.

$$C_3H_8 = \dot{C}H_3 + \dot{C}_2H_5 \quad (413)$$

$$C_3H_8 + \dot{H} = i\dot{C}_3H_7 + H_2 \quad (418)$$

$$C_3H_8 + \dot{H} = n\dot{C}_3H_7 + H_2 \quad (419)$$

$$C_3H_8 + \dot{C}H_3 = i\dot{C}_3H_7 + CH_4 \quad (426)$$

$$C_3H_8 + \dot{C}H_3 = n\dot{C}_3H_7 + CH_4 \quad (427)$$

Propene is principally produced via unimolecular decomposition of *iso*- and *n*-propyl radicals produced by the reactions 418, 419, 426, and 427. The methyl radical addition reaction to ethylene, and methyl and vinyl radical recombination reactions also produce propene, which decomposes mainly via unimolecular decomposition reactions and hydrogen abstraction reactions, mainly by $\dot{H}$ atom and $\dot{C}H_3$ radical.

$$i\dot{C}_3H_7 = C_3H_6 + \dot{H} \quad (449)$$

$$n\dot{C}_3H_7 = C_3H_6 + \dot{H} \quad (456)$$

$$\dot{C}_2H_3 + \dot{C}H_3(+M) = C_3H_6(+M) \quad (461)$$

$$C_3H_6 + \dot{H} = \dot{C}_3H_5\text{-a} + H_2 \quad (477)$$

$$C_3H_6 + \dot{H} = \dot{C}_3H_5\text{-s} + H_2 \quad (478)$$

$$C_3H_6 + \dot{H} = \dot{C}_3H_5\text{-t} + H_2 \quad (479)$$

$$C_3H_6 + \dot{H} = C_2H_4 + \dot{C}H_3 \quad (480)$$

$$C_3H_6 + \dot{C}H_3 = \dot{C}_3H_5\text{-a} + CH_4 \quad (484)$$

Allene is mainly produced via unimolecular decomposition of C_3H_5-a and C_3H_5-t radicals produced by reactions 477, 479, and 484, and it decomposes mainly via hydrogen abstraction reactions principally by $\dot{H}$ atom.

$$\dot{C}_3H_5\text{-a} = C_3H_4\text{-a} + \dot{H} \quad (498)$$

$$\dot{C}_3H_5\text{-t} = C_3H_4\text{-a} + \dot{H} \quad (517)$$

$$C_3H_4\text{-a} + \dot{H} = \dot{C}_3H_3 + H_2 \quad (532)$$

Propyne is principally produced via unimolecular decomposition of C_3H_5-s and C_3H_5-t radicals produced by the reactions 478 and 479, and decomposes mainly via hydrogen abstraction reactions principally by $\dot{H}$ atom.

$$\dot{C}_3H_5\text{-s} = C_3H_4\text{-p} + \dot{H} \quad (512)$$

$$\dot{C}_3H_5\text{-t} = C_3H_4\text{-p} + \dot{H} \quad (518)$$

$$C_3H_4\text{-p} + \dot{H} = \dot{C}_3H_3 + H_2 \quad (547)$$

Methane is mainly produced via hydrogen abstraction by methyl radical from formaldehyde, hydrogen molecule, acetaldehyde (211), ethylene (252), ethanol (301) and (302), and DEE (677) and (678). Here, formaldehyde is produced via unimolecular decomposition of hydroxy-methyl radical, ethoxy and $C_2H_5OCH_2$ radicals.

$$CH_2O + \dot{C}H_3 = H\dot{C}O + CH_4 \quad (46)$$

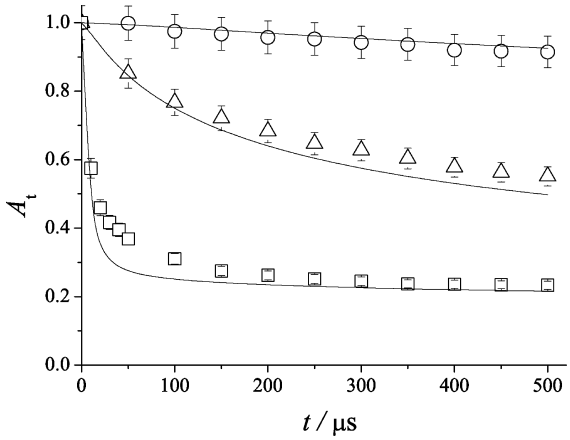

Figure 3. IR absorption profiles at 3.39 μm from LAST for 2.0% DEE diluted in Ar, lines simulation and symbols experiment. Fuel (DEE) and products which have C−H bond absorb light at this wavelength. ○, T_5 = 1158 K, P_5 = 1.7 atm; Δ, T_5 = 1314 K, P_5 = 2.2 atm; □, T_5 = 1589 K, P_5 = 3.0 atm.

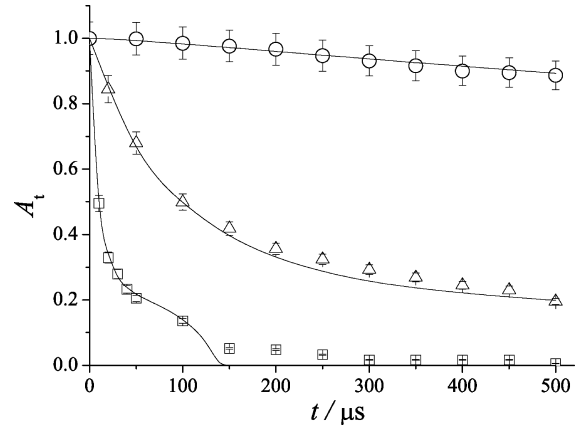

Figure 4. IR absorption profiles at 3.39 μm from LAST for 1.0% DEE and 3.0% O_2 diluted in Ar, ϕ = 2.0, lines simulation and symbols experiment. Fuel (DEE) and products which have C−H bond absorb light at this wavelength. ○, T_5 = 1173 K, P_5 = 1.5 atm; Δ, T_5 = 1363 K, P_5 = 1.9 atm; □, T_5 = 1589 K, P_5 = 2.3 atm.

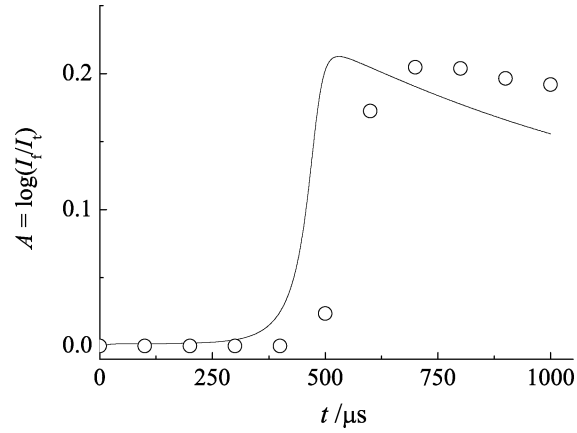

Figure 5. UV absorption profile at 306.7 nm from UAST for 0.1% DEE, 1.0% H_2, and 1.0% O_2 diluted in Ar; line is simulation and symbols are experiment. OH radical absorbs light at this wavelength. T_5 = 1339 K, P_5 = 1.6 atm.

$$CH_4 + \dot{H} = \dot{C}H_3 + H_2 \quad (99)$$

$$CH_2O + \dot{H}(+M) = \dot{C}H_2OH(+M) \quad (70)$$

$$C_2H_5\dot{O} = \dot{C}H_3 + CH_2O \quad (174)$$

$$C_2H_5OCH_2 = \dot{C}_2H_5 + CH_2O \quad (749)$$

Carbon monoxide is principally produced via formyl and acetyl radical decompositions. Acetyl radical is produced via hydrogen abstraction reaction from acetaldehyde by $\dot{H}$ atom, reaction 207 and $\dot{C}H_3$ radical, reaction 211 and unimolecular decomposition of acetaldehyde, reaction (206).

$$H\dot{C}O + M = H + CO + M \quad (26)$$

$$CH_3CO\,(+M) = \dot{C}H_3 + CO\,(+M) \quad (217)$$

Acetylene is mainly produced via vinyl radical decomposition. Vinyl radical is produced via reactions 248 and 252.

$$\dot{C}_2H_3(+M) = C_2H_2 + \dot{H}(+M) \quad (263)$$

Time-Resolved IR-Laser Absorption at 3.39 μm. The wavelength at 3.39 μm corresponds to the asymmetric C−H bond stretch, so that fuel (DEE) and products that have a C−H bond absorb light at this wavelength. Three typical absorption profiles measured by using LAST for 2% DEE diluted with argon are shown in Figure 3. At temperatures below 1000 K, the absorption intensities after the rapid rise at the reflected shock front remained constant for about 1000 μs. At temperatures above 1000 K, the absorption intensities after the rapid rise slowly decreased with time. The model captures the behavior of time dependence of absorption profiles for pyrolysis very well.

Oxidation. ***Time-Resolved IR-Laser Absorption at 3.39 μm.*** The wavelength at 3.39 μm corresponds to the asymmetric C−H bond stretch, so that fuel (DEE) and products that have a C−H bond absorb light at this wavelength. Three typical absorption profiles measured by using LAST for 1% DEE and 3% oxygen diluted with argon are shown in Figure 4. At temperatures below 1000 K, the absorption intensities after the rapid rise at the reflected shock front remained constant for about 1000 μs. At temperatures above 1000 K, the absorption intensities after the rapid rise slowly decreased with time. The model also captures the behavior of time dependence of absorption profiles for oxidation very well.

Time-Resolved OH Absorption at 306.7 nm. $\dot{O}H$ radicals absorb light at 306.7 nm. The absorption profiles at 306.7 nm were measured for 0.1% DEE, 1.0% O_2, 1.0% H_2 diluted with argon in the pressure range 1.6−2.1 atm by using UAST. Small amount of DEE was added to the 1.0% H_2 and 1.0% O_2 to measure the inhibition effect of DEE. A typical absorbance profile at 306.7 nm is shown in Figure 5. The profile exhibits a rapid increase after a period following shock heating and decreases gradually. After rapid increase of $\dot{O}H$ radicals, $\dot{O}H$ radicals are consumed by the following reactions, $\dot{O}H + H_2 = \dot{H} + H_2O$, $H_2O + M = \dot{H} + \dot{O}H + M$ and $CO + \dot{O}H = CO_2 + \dot{H}$, so that absorbance profile decrease after ignition. Simulation captures the time dependent behavior of UV absorption profile at 306.7 nm very well. An induction time τ_{OH} was defined as the elapsed time between reflected shock arrival and the onset of the rapid absorption increase, determined from the intersection of the tangent to the curve at its inflection point with the

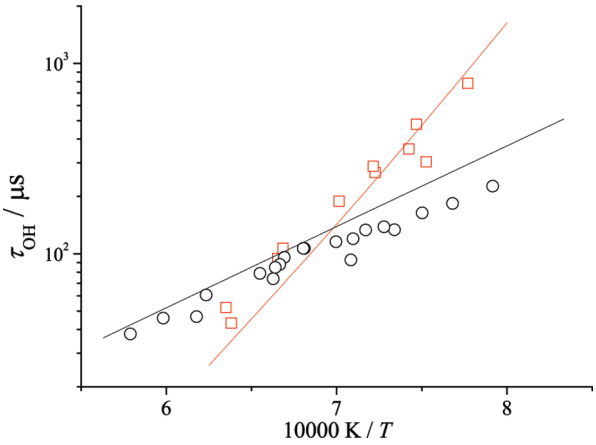

Figure 6. Temperature dependence of τ_{OH} from UAST; lines are simulation and symbols are experiment. □, 0.1% DEE, 1.0% O_2, and 1.0% H_2 diluted in Ar; ○, 1.0% O_2 and 1.0% H_2 diluted in Ar at 1.4−2.3 atm.

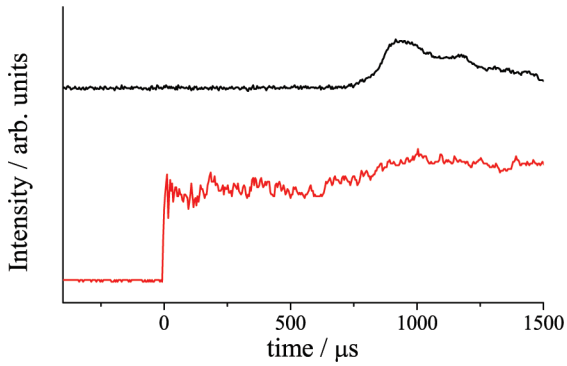

Figure 7. Profiles for UV emission at 431 nm and pressure from UEST for 1.0% DEE, 12.0% O_2, $\phi = 0.5$, diluted in Ar, upper line emission and lower line pressure. Exited CH* radical emits light at this wavelength. $T_5 = 1430$ K, $P_5 = 1.1$ atm.

preshock baseline. The induction period τ_{OH} observed is shown in Figure 6 together with the results of oxidation of a mixture of 1% H_2, 1% O_2 diluted with argon. τ_{OH} were estimated within 5% uncertainty. It was found that ȮH radical formation was inhibited by the addition of DEE under our experimental conditions below about 1500 K, as shown in Figure 6. The model captures well the temperature dependence of τ_{OH}.

Time-Resolved UV-Emission at 431 nm. UV emission at 431 nm corresponds to the emission from exited CH* radical, which is produced by the following reaction, $\dot{C}_2H + \ddot{O} = CH^* + CO$. UV emission profiles at 431 nm were measured for mixtures B: (1.0% DEE, 3.0% O_2 diluted with argon), C: (1.0% DEE, 6.0% O_2 diluted with argon), and D: (1.0% DEE, 12.0% O_2 diluted with argon) by using the UEST. Typical emission and pressure profiles are shown in Figure 7. Significant pressure rise was not observed under our experimental conditions. The ignition delay time was defined as the interval between the rise in the pressure due to the arrival of the shock wave at the end wall and the maximum rate of rise of the emission signal.

Ignition Delay. Figure 8, panels a and b, depicts the effect of equivalence ratio on ignition delay time for 1.0% DEE/oxygen mixtures at average pressures of 1 and 3.5 atm, respectively. At both pressures, we observe the high negative dependence[47,48] of ignition time on oxygen concentration which is observed at high temperatures ($1250 \leq T \leq 1850$ K) for almost all hydrocarbon and oxygenated hydrocarbon fuels. Figure 9, panels a and b, depicts the effect of pressure on ignition delay times for $\phi = 0.5$ and 2.0, at average pressures of 1.0 and 3.5 atm, respectively. It can be observed that as the pressure increases, which is an effective increase in concentration, the ignition delay time becomes faster. The predicted ignition delays agree well with measured values for lean to rich conditions. The model captures well the dependence on increasing oxygen concentration and pressure.

Sensitivity and Reaction Path Analysis. ***Pyrolysis.*** Sensitivity analyses were carried out to investigate the dependence of the important reactions to the concentrations of DEE and products, and A_t profile for DEE pyrolysis. The analyses were carried out by increasing and decreasing both the forward and reverse rate constants by a factor of 2, with sensitivities expressed using the formula: Sensitivity = (log (factor$_+$/factor$_-$))/(log (k_+/k_-)) = (log (factor$_+$/factor$_-$))/(log (2/0.5)). Where, "factor" denotes concentration of species, or absorbance, or ignition time, etc.

Figure 10 depicts the sensitivity coefficients of species concentrations for a 2% DEE pyrolysis at 1300 K, 2.0 atm and 1.5 ms corresponding to SPST and conditions in Figure 2. A positive sensitivity indicates an increase in the species concentrations, conversely a negative value indicates a decrease in the species concentrations. The primary DEE reactions have strong negative sensitivities to DEE concentration. Hydrogen atom abstraction by hydrogen atoms from DEE at the α-position producing $C_2H_5O\dot{C}_2H_4$-s has a strong positive sensitivity to acetaldehyde concentration, while hydrogen atom abstraction by hydrogen atoms from the α-position on acetaldehyde has a strong negative sensitivity.

The unimolecular elimination reaction of DEE has a very strong positive sensitivity to ethanol concentration. The methyl radical recombination reaction to form ethane and the ethoxy

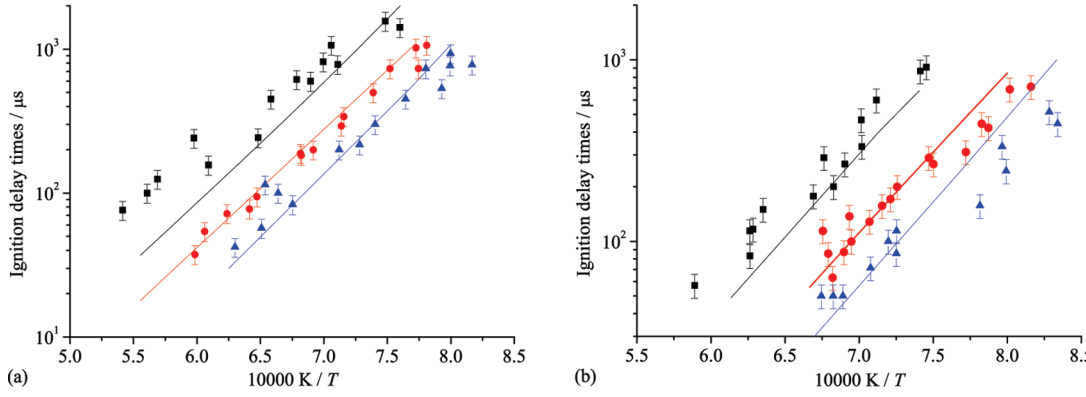

Figure 8. Influence of equivalence ratio on ignition delay times from UEST at 1.0% DEE in Ar; lines are simulation and symbols are experiment. (a) $P_5 = 1.0$ atm, (b) $P_5 = 3.5$ atm, ■, $\phi = 2.0$, 3% O_2; ●, $\phi = 1.0$, 6% O_2; ▲, $\phi = 0.5$, 12% O_2.

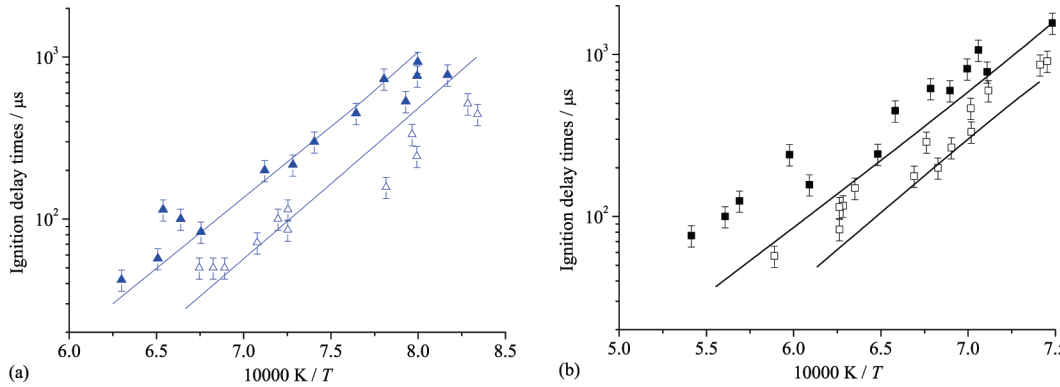

Figure 9. Influence of pressure on ignition delay times from UEST at 1.0% DEE in Ar; lines are simulation and symbols are experiment. (a) $\phi = 0.5$ (12% O_2), (b) $\phi = 2.0$ (3% O_2), solid symbols: $p_5 = 1.0$ atm, open symbols: $p_5 = 3.5$ atm.

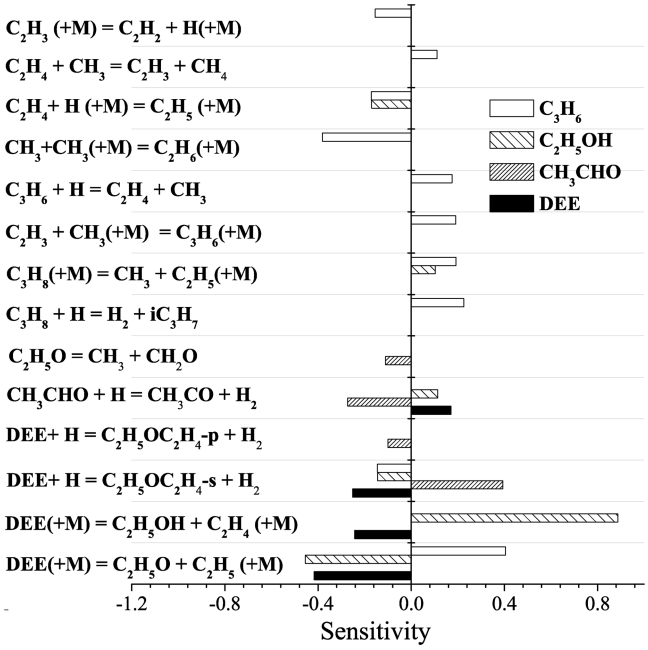

Figure 10. Sensitivity to species concentration; 2% DEE diluted in Ar, 1300 K, 2.0 atm, $t_e = 1500$ μs, corresponding to SPST and conditions in Figure 2.

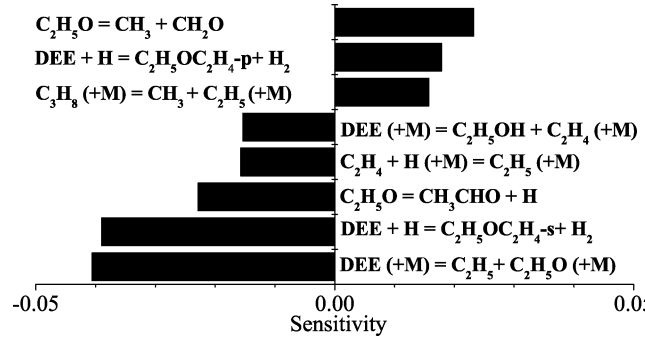

Figure 11. Sensitivity to A_t; 2% DEE diluted in Ar, 1314 K, 2.2 atm, and 50 μs, corresponding to LAST conditions in Figure 3.

radical decomposition to form a methyl radical and formaldehyde have negative sensitivities to propene concentration, whereas the simple C−C and C−O bond fission reactions of DEE, ethenyl, and methyl radicals recombination reactions to form propene and hydrogen atom addition reaction to propene to form ethylene and a methyl radical have a negative sensitivity to propene concentration.

Figure 11 depicts sensitivity coefficients of the A_t profile for a 2% DEE pyrolysis at 1314 K, 2.2 atm, and 50 μs, corresponding to LAST and conditions in Figure 3. A positive sensitivity indicates an increase in the value of A_t, conversely negative value indicates a decrease in the value of A_t. The unimolecular decomposition reactions of DEE, hydrogen atom abstraction reactions from DEE by hydrogen atoms at the α-position and ethoxy radical decomposition to form a hydrogen atom and acetaldehyde have strong negative sensitivities. Hydrogen atom abstraction by hydrogen atoms from DEE at the β-position and ethoxy radical decomposition to form a methyl radical and formaldehyde all have positive sensitivities.

A reaction path analysis was carried out for the shock tube conditions outlined in Figure 12. The reaction scheme shows that the DEE undergoes the four-centered elimination to ethanol and ethylene, simple C−C and C−O bond fission, and hydrogen atom abstraction producing $C_2H_5O\dot{C}_2H_4$-p and $C_2H_5O\dot{C}_2H_4$-s radicals, which accounts for 12.2, 1.2, 15.9, 16.2, and 54.3% of total DEE consumed, respectively. The $C_2H_5O\dot{C}_2H_4$-p radical undergoes β−scission to form ethylene and an ethoxy radical. The $C_2H_5O\dot{C}_2H_4$-s radical also undergoes β−scission to form acetaldehyde and an ethyl radical. Ethanol, observed in the pyrolysis of DEE, is only produced from the four-centered elimination reaction. Ethoxy radical has two decomposition channels (174) and (175),

$$C_2H_5\dot{O} = \dot{C}H_3 + CH_2O \quad (174)$$

$$C_2H_5\dot{O} = CH_3CHO + \dot{H} \quad (175)$$

reaction 174 produces methyl radical, whereas reaction 175 produces relatively active hydrogen atom comparing to methyl radical so that the branching ratio of ethoxy radical decomposition plays an important role in the reactivity of DEE pyrolysis.

Oxidation. Sensitivity analyses were carried out to investigate reaction sensitivity to the A_t profile, τ_{OH}, and ignition time for DEE oxidation. Figure 13 depicts sensitivity coefficients of the A_t profile for a 1% DEE and 3% O_2 with Ar at 1363 K, 1.9 atm and 50 μs, corresponding to LAST and conditions in Figure 4. A positive sensitivity indicates an increase in the value of A_t; conversely, a negative value indicates a decrease in its value. Here we see similar trends to those observed for pyrolysis. At the early stage of reaction, the rate constants for the primary reactions of DEE involving unimolecular decomposition and hydrogen atom abstraction and ethoxy-ethyl radical decomposition reactions have the largest influence on the consumption of DEE whether oxygen molecules are present or not. Species that

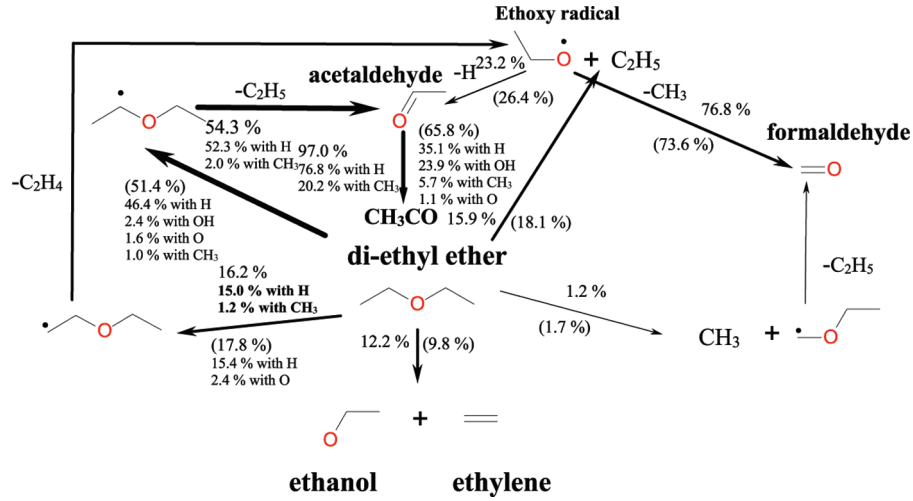

Figure 12. Reaction path analysis for DEE pyrolysis and oxidation. Shock conditions: Pyrolysis, 2% DEE diluted in Ar, 1300 K, 2.0 atm, 20% consumption; Oxidation, 1% DEE and 6% O_2 in Ar, $\phi = 1.0$, 1400 K, 3.5 atm, 20% consumption. The numbers with and without parentheses are in the cases of pyrolysis and oxidation, respectively.

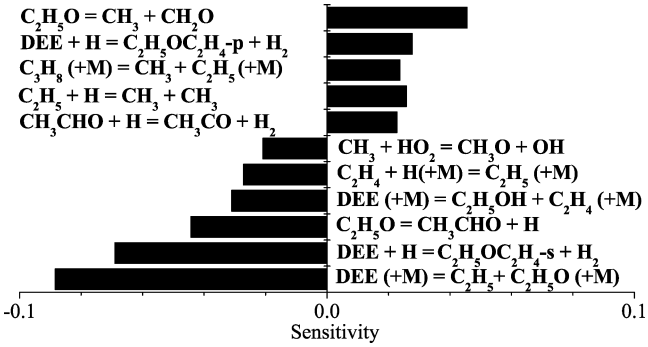

Figure 13. Sensitivity to A_t; 1% DEE, 3% O_2 diluted in Ar, 1363 K, 1.9 atm, and 50 μs, corresponding to LAST and conditions in Figure 4.

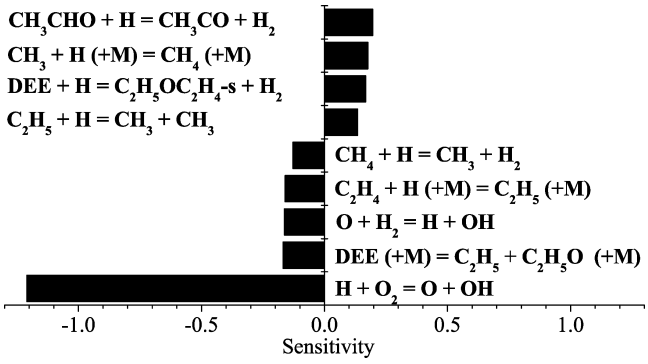

Figure 14. Sensitivity to τ_{OH}; 0.1% DEE, 1% O_2, and 1% H_2 diluted in Ar, 1339 K, 1.6 atm, corresponding to UAST and conditions in Figure 5.

have C−H bonds absorbs light at 3.39 μm, and being the fuel, DEE is the strongest absorber under our experimental conditions, thus the primary reactions of DEE show a strong sensitivity to the A_t profiles.

Figure 14 depicts sensitivity coefficients of τ_{OH} for a 0.1% DEE, 1% H_2, and 1% O_2 with Ar at 1339 K and 1.9 atm, corresponding to UAST and conditions in Figure 5. A positive sensitivity indicates an increase in the value of τ_{OH}, conversely a negative value indicates a decrease in the value of τ_{OH}. The radical branching reaction, $\dot{H} + O_2 = \ddot{O} + \dot{O}H$, has a very strong negative sensitivity. The reactions which consume $\dot{H}$ atoms, competing with this chain branching reaction, have a positive sensitivity and inhibit reactivity.

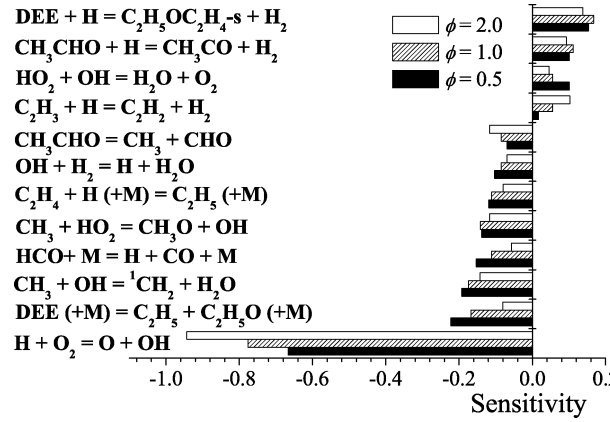

Figure 15. Sensitivity coefficients showing the effect of equivalence ratio on ignition time, for 1% DEE, 1550 K and 1.0 atm, corresponding to UEST and conditions of ■, ●, and ▲ in Figure 8a.

Figure 15 depicts sensitivity coefficients as a function of equivalence ratio for mixtures B, C, and D at 1450 K and a pressure of 1.0 atm, corresponding to UEST and conditions in Figure 8a. We see higher sensitivity coefficients to the C−C bond fission of DEE for the lean condition compared to stoichiometric, whereas under rich conditions we observe the lowest sensitivity. Hydrogen abstraction reactions from DEE and acetaldehyde show a negative sensitivity for all mixtures. As it was also seen for sensitivity to τ_{OH}, these reactions inhibit the oxidation of DEE.

Figure 16 depicts sensitivity coefficients as a function of pressure for mixture C at 1550 K corresponding to UEST and conditions of in Figure 8a and b. Sensitivity coefficients at both pressures do not show large differences.

Figure 17 depicts sensitivity coefficients as a function of temperature for mixture D at 3.5 atm corresponding to UEST and conditions of in Figure 8a. The radical branching reaction, $\dot{H} + O_2 = \ddot{O} + \dot{O}H$, has a higher value at 1450 K than at 1200 K. However, C−O bond fission of DEE, DEE(+M) = C_2H_5 + C_2H_5O (+M), and methyl and hydroperoxy radicals reaction to produce methoxy and hydroxy radicals have higher values at 1200 K than 1450 K.

A reaction path analysis was carried out for the shock tube conditions outlined in Figure 12. The reaction proceeds basically in the same way as pyrolysis, the main difference being the

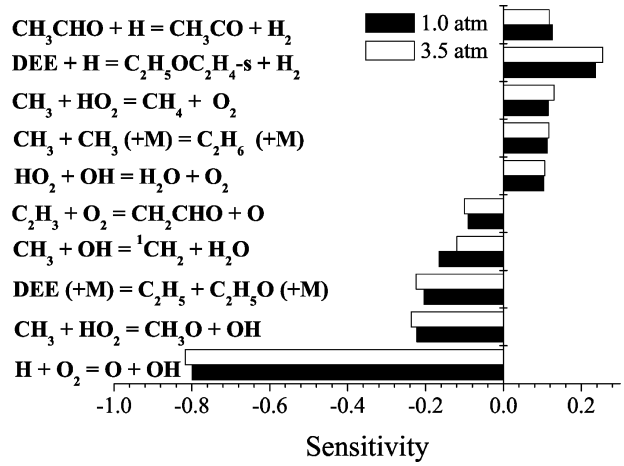

Figure 16. Sensitivity coefficients showing the effect of pressure on DEE ignition time, 1450 K and $\phi = 1$ (1.0% DEE and 6% O_2 diluted in Ar), corresponding to UEST and conditions of ● in Figure 8a and b.

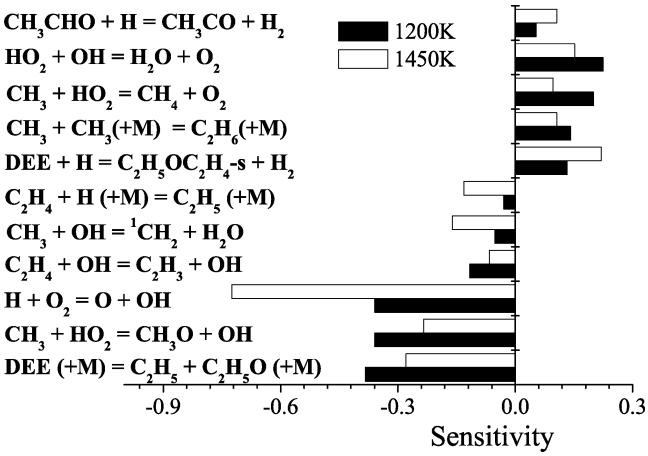

Figure 17. Sensitivity coefficients showing the effect of temperature on DEE ignition time, 3.5 atm, and $\phi = 0.5$ (1.0% DEE and 12.0% O_2 diluted in Ar), corresponding to UEST and conditions of ▲ in Figure 8b.

contribution of ȮH radical and Ö atoms to the overall reactivity. 51.4% of DEE is consumed via hydrogen atom abstraction from the α−position of DEE by Ḣ and Ö atoms, and by $\dot{C}H_3$ and ȮH radicals to produce the $C_2H_5O\dot{C}_2H_4$-s radical which subsequently decomposes to produce acetaldehyde and an ethyl radical. Acetaldehyde reacts with hydrogen atoms to produce acetyl and hydrogen molecule. Ethyl radical decomposes to produce ethylene and a hydrogen atom. DEE reacts with relatively reactive Ḣ and Ö atoms and ȮH radical to convert relatively inactive methyl radical through the reactions described above. Thus, hydrogen atom abstraction reactions from DEE inhibits the reactivity of the system.

Conclusions

A comprehensive set of experiments in four different shock tubes has generated a wealth of data describing the thermal decomposition and oxidation of diethyl ether. Thus, species profiles for ethanol, acetaldehyde, propane, propene, ethane, ethylene, acetylene, allene, propyne, methane, as well as carbon monoxide were obtained in the SPST by GC for 2% DEE in argon at pressures 1−3.1 atm and for dwell times of 1.2−1.8 ms.

Time-resolved IR absorption profiles at 3.39 μm, which is dominated principally by molecules with C−H stretching vibrations near 3000 cm^{-1}, was used to track the concentration of DEE in pyrolysis and oxidation experiments. Furthermore, time-resolved UV absorption at 306.7 nm was used to determine the concentration of the ȮH radical in oxidation experiments.

Autoignition delay times were measured to determine the influence of pressure and stoichiometry of DEE oxygen mixtures. Typical behavior was observed; increasing the pressure reduces the ignition delay time, whereas increasing the oxygen concentration at a constant DEE concentration reduces the ignition delay.

A detailed chemical kinetics model was assembled from a base mechanism of the recent natural gas,[37−42] *n*-butane,[43] and *iso*-butane[44] mechanisms, and their blends[45] and reactions specific to diethyl ether were added. The final model consists of 751 reversible reactions between 148 species. The entropy of DEE has a considerable influence on the results; the value of 81.8 cal mol^{-1} K^{-1}, which was taken from the recommendation of the NIST database,[25] provides a better fit to our experiments.

The most important reactions of DEE include the four-centered elimination, DEE = $C_2H_5OH + C_2H_4$, C−O bond fission, DEE = $C_2H_5\dot{O} + \dot{C}_2H_5$, and the hydrogen atom abstraction reactions by hydrogen atoms primarily to the secondary radical $C_2H_5O\dot{C}_2H_4$ -s. This in turn eliminates an ethyl radical to form acetaldehyde.

Acknowledgment. We would like to acknowledge the support of Science Foundation Ireland under grant No. 08/IN.1/I2055 through their Principal Investigator Awards.

Supporting Information Available: The detailed chemical kinetic mechanism and thermochemical data are available as Supporting Information. This material is available free of charge via the Internet at http://pubs.acs.org.

Note Added after ASAP Publication. This article posted ASAP on August 6, 2010. Equation 217 has been revised. The correct version posted on August 12, 2010.

References and Notes

(1) Bailey, B.; Eberhardt, J.; Goguen, S.; Erwin, J. *SAE Technical Paper 972978* 1997.

(2) Erwin, J.; Moulton, S., Maintenance and Operation of the U.S. DOE Alternative Fuel Center. Subcontract XS-2−12130−1. San Antonio, TX: Southwest Research Institute, Project No. 01−5151. November, 1996.

(3) Laidler, J. K.; McKenney, J. D. *Proc. Royal Soc. A* **1964**, *278*, 505–516.

(4) Laidler, J. K.; McKenney, J. D. *Proc. Royal Soc. A* **1964**, *278*, 517–526.

(5) Seres, I.; Huhn, P. *Magy. Kem. Foly.* **1975**, *81*, 120–123.

(6) Foucaut, J. F.; Martin, R. *J. Chim. Phys.* **1978**, *75*, 132–144.

(7) Waddington, D. J. *Proc. Royal Soc. A* **1959**, *252*, 260–272.

(8) Tranter, R. S.; Walker, R. W. *Phys. Chem. Chem. Phys.* **2001**, *3*, 4722–4732.

(9) Ogura, T.; Miyoshi, A.; Koshi, M. *Phys. Chem. Chem. Phys.* **2007**, *9*, 5133–5142.

(10) Zhang, N.; Di, Y. G.; Huang, Z. H.; Zhang, Z. Y. *Chin. Sci. Bull.* **2010**, *55*, 314–320.

(11) Zhang, N.; Di, Y. G.; Huang, Z. H.; Zheng, B.; Zhang, Z. Y. *Energy Fuels* **2009**, *23*, 5798–5805.

(12) Cinar, C.; Can, O.; Sahin, F.; Yuces, H. S. *Appl. Therm. Eng.* **2010**, *30*, 360–365.

(13) Di, Y. G.; Huang, Z. H.; Zhang, N.; Zheng, B.; Wu, X. S.; Zhang, Z. Y. *Energy Fuel* **2009**, *23*, 2490–2497.

(14) Jothi, N. K. M.; Nagarajan, G.; Renganarayanan, S. *Int. J. Therm. Sci.* **2010**, *30*, 360–365.

(15) Morley, C. Gaseq v0.79; Available from http://www.arcl02.dsl.pipex.com/gseqrite.htm.

(16) Hidaka, Y.; Shiba, S.; Takuma, H.; Suga, M. *Int. J. Chem. Kinet.* **1985**, *17*, 441–453.

(17) Hidaka, Y.; Nakamura, T.; Miyauchi, A.; Shiraishi, T.; Kawano, H. *Int. J. Chem. Kinet.* **1989**, *21*, 643–666.
(18) Hidaka, Y.; Hattori, K.; Okuno, T.; Inami, K.; Abe, T.; Koike, T. *Combust. Flame* **1996**, *107*, 401–417.
(19) Hidaka, Y.; Kimura, K.; Hattori, K.; Okuno, T. *Combust. Flame* **1996**, *106*, 155–167.
(20) Hidaka, Y.; Taniguchi, T.; Tanaka, H.; Kamesawa, T.; Inami, K.; Kawano, H. *Combust. Flame* **1993**, *92*, 365–376.
(21) Hidaka, Y.; Higashihara, T.; Nishimori, T.; Sato, K.; Henmi, Y.; Okuda, R.; K. Inami, K. *Combust. Flame* **1999**, *117*, 755–776.
(22) Hidaka, Y.; Higashihara, T.; Nishimori, N.; Oshita, H.; Kawano, H. *J. Phys. Chem.* **1993**, *97*, 10977–10983.
(23) Ritter, E. R.; Bozzelli, J. W. *Int. J. Chem. Kinet.* **1991**, *23*, 767–778.
(24) Benson, S. W. *Thermochemical Kinetics: Methods for the Estimation of Thermochemical Data and Rate Parameters*, 2nd ed; Wiley: New Yorkc 1976.
(25) Stein, S. E.; Brown, R. L. In *Structure and Properties Group Additivity Model in NIST Chemistry Webbook*; Linstrom, J. P., Mallards, G. W., Eds.; NIST standard reference database number 69, June 2005; National Institute of Standards and Technology: Gaithersburg MD, 20899. uri: http://webbook.nist.gov.
(26) Fisher, S. L.; Dryer, F. L.; Curran, H. J. *Int. J. Chem. Kinet.* **2000**, *32*, 713–740.
(27) Tsang, W. *J. Phys. Chem. Ref. Data* **1988**, *17*, 887–952.
(28) Yasunaga, K.; Kuraguchi, Y.; Hidaka, Y.; Takahashi, O.; Yamada, H.; Koike, T. *Chem. Phys. Lett.* **2007**, *451*, 192–197.
(29) Frisch, M. J., Trucks, G. W.; Schlegel, H. B.; Scuseria, G. E.; Robb, M. A.; Cheeseman, J. R.; Montgomery, J. A., Jr., ; Vreven, T.; Kudin, K. N.; Burant, J. C.; Millam, J. M.; Iyengar, S. S.; Tomasi, J.; Barone, V.; Mennucci, B.; Cossi, M.; Scalmani, G.; Rega, N.; Petersson, G. A.; Nakatsuji, H.; Hada, M.; Ehara, M.; Toyota, K.; Fukuda, R.; Hasegawa, J.; Ishida, M.; Nakajima, T.; Honda, Y.; Kitao, O.; Nakai, H.; Klene, M.; Li, X.; Knox, J. E.; Hratchian, H. P.; Cross, J. B.; Bakken, V.; Adamo, C.; Jaramillo, J.; Gomperts, R.; Stratmann, R. E.; Yazyev, O.; Austin, A. J.; Cammi, R.; Pomelli, C.; Ochterski, J. W.; Ayala, P. Y.; Morokuma, K.; Voth, G. A.; Salvador, P.; Dannenberg, J. J.; Zakrzewski, V. G.; Dapprich, S.; Daniels, A. D.; Strain, M. C.; Farkas, O.; Malick, D. K.; Rabuck, A. D.; Raghavachari, K.; Foresman, J. B.; Ortiz, J. V.; Cui, Q.; Baboul, A. G.; Clifford, S.; Cioslowski, J.; Stefanov, B. B.; Liu, G.; Liashenko, A.; Piskorz, P.; Komaromi, I.; Martin, R. L.; Fox, D. J.; Keith, T.; Al-Laham, M. A.; Peng, C. Y.; Nanayakkara, A.; Challacombe, M.; Gill, P. M. W.; Johnson, B.; Chen, W.; Wong, M. W.; Gonzalez, C.; and Pople, J. A. *Gaussian 03, Revision C.02*; Gaussian, Inc.: Wallingford, CT, 2004.
(30) Dean, A. M. *J. Phys. Chem.* **1985**, *89*, 4600–4608.
(31) Dean, A. M. *Combust. Sci. Technol.* **1991**, *80*, 63–85.
(32) Gilbert, R. G.; Luther, K.; Troe, J. *Ber Bunsenges. Phys. Chem.* **1983**, *87*, 169–177.
(33) Zhou, C.; Simmie, J. M.; Curran, H. J. *Phys. Chem. Chem. Phys.* **2010**, *12*, 7221–7233.
(34) Orme, J. P.; Curran, H. J.; Simmie, J. M. *J. Phys. Chem. A* **2006**, *110*, 114–131.
(35) Curran, H. J. *Int. J. Chem. Kinet.* **2006**, *38*, 250–275.
(36) Bentz, T.; Striebel, F.; Olzmann, M. *J. Phys. Chem. A* **2008**, *112*, 6120–6124.
(37) Petersen, E. L.; Kalitan, D. M.; Simmons, S.; Bourque, G.; Curran, H. J.; Simmie, J. M. *Proc. Combust. Inst.* **2007**, *31*, 447–454.
(38) Gallagher, S.; Curran, H. J.; Metcalfe, W. K.; Healy, D.; Simmie, J. M.; Bourque, G. *Combust. Flame* **2007**, *153*, 316–333.
(39) Healy, D.; Curran, H. J.; Dooley, S.; Simmie, J. M.; Kalitan, D. M.; Petersen, E. L.; Bourque, G. *Combust. Flame* **2008**, *155*, 451–461.
(40) Healy, D.; Curran, H. J.; Simmie, J. M.; Kalitan, D. M.; Zinner, C. M.; Barrett, A. B.; Petersen, E. L.; Bourque, G. *Combust. Flame* **2008**, *155*, 441–448.
(41) Healy, D.; Kopp, M. M.; Polley, N. L.; Petersen, E. L.; Bourque, G.; Curran, H. J. *Energy Fuels* **2010**, *24* (3), 1617–1627.
(42) Healy, D.; Kalitan, D. M.; Aul, C. J.; Petersen, E. L.; Bourque, G.; Curran, H. J. *Energy Fuels* **2010**, *24* (3), 1521–1528.
(43) Healy, D.; Donato, N. S.; Aul, C. J.; Petersen, E. L.; Zinner, C. M.; Bourque, G.; Curran, H. J. *Combust. Flame* **2010**, *157*, 1526–1539.
(44) Healy, D.; Donato, N. S.; Aul, C. J.; Petersen, E. L.; Zinner, C. M.; Bourque, G.; Curran, H. J. *Combust. Flame* **2010**, *157*, 1540–1551.
(45) Donato, N.; Aul, C.; Petersen, E.; Zinner, C.; Curran, H.; Bourque, G. *J. Eng. Gas Turb. Power* **2010**, *132* (5), 051502.
(46) Chemkin-Pro; Reaction Design Inc.: San Diego, California, USA.
(47) Horning, D. C.; Davidson, D. F.; Hanson, R. K. *J. Prop. Power* **2002**, *18*, 363–371.
(48) Smith, J. M.; Simmie, J. M.; Curran, H. J. *Int. J. Chem. Kinet* **2005**, *37*, 728–736.

JP104070A